



Short communication

Design, synthesis and crystallographic analysis of nitrile-based broad-spectrum peptidomimetic inhibitors for coronavirus 3C-like proteases

Chi-Pang Chuck^a, Chao Chen^b, Zhihai Ke^b, David Chi-Cheong Wan^c, Hak-Fun Chow^b, Kam-Bo Wong^{a,*}^aSchool of Life Sciences and Center for Protein Science and Crystallography, The Chinese University of Hong Kong, Shatin, Hong Kong^bDepartment of Chemistry, State Key Laboratory of Synthetic Chemistry, and Center of Novel Functional Molecules, The Chinese University of Hong Kong, Shatin, Hong Kong^cSchool of Biomedical Sciences, The Chinese University of Hong Kong, Shatin, Hong Kong

ARTICLE INFO

Article history:

Received 19 September 2012

Received in revised form

29 October 2012

Accepted 31 October 2012

Available online 7 November 2012

Keywords:

Peptidomimetics

Coronavirus

X-ray crystallography

Protease

ABSTRACT

Coronaviral infection is associated with up to 5% of respiratory tract diseases. The 3C-like protease (3CL^{pro}) of coronaviruses is required for proteolytic processing of polyproteins and viral replication, and is a promising target for the development of drugs against coronaviral infection. We designed and synthesized four nitrile-based peptidomimetic inhibitors with different N-terminal protective groups and different peptide length, and examined their inhibitory effect on the *in-vitro* enzymatic activity of 3CL^{pro} of severe-acute-respiratory-syndrome-coronavirus. The IC₅₀ values of the inhibitors were in the range of 4.6–49 μM, demonstrating that the nitrile warhead can effectively inactivate the 3CL^{pro} auto-cleavage process. The best inhibitor, Cbz-AVLQ-CN with an N-terminal carbobenzyloxy group, was ~10x more potent than the other inhibitors tested. Crystal structures of the enzyme–inhibitor complexes showed that the nitrile warhead inhibits 3CL^{pro} by forming a covalent bond with the catalytic Cys145 residue, while the AVLQ peptide forms a number of favourable interactions with the S1–S4 substrate-binding pockets. We have further showed that the peptidomimetic inhibitor, Cbz-AVLQ-CN, has broad-spectrum inhibition against 3CL^{pro} from human coronavirus strains 229E, NL63, OC43, HKU1, and infectious bronchitis virus, with IC₅₀ values ranging from 1.3 to 3.7 μM, but no detectable inhibition against caspase-3. In summary, we have shown that the nitrile-based peptidomimetic inhibitors are effective against 3CL^{pro}, and they inhibit 3CL^{pro} from a broad range of coronaviruses. Our results provide further insights into the future design of drugs that could serve as a first line defence against coronaviral infection.

© 2012 Elsevier Masson SAS. All rights reserved.

1. Introduction

Coronaviruses (CoVs) cause a number of respiratory tract and gastroenteritis diseases in human and animals [1]. Coronaviruses can be classified into three main groups: alphacoronavirus (group 1), betacoronavirus (group 2), and gammacoronavirus (group 3), while the group 2 is further sub-divided into group 2a and 2b [2]. In addition to the SARS-CoV (group 2b) that caused the outbreak of pneumonia in 2003, the four human group 1 (229E and NL63) and 2 (OC43 and HKU1) strains are associated with up to 5% of respiratory tract disease cases reported [3,4]. The single-stranded RNA genome of CoVs encodes two polyproteins, which are processed into at least 15 mature proteins by papain-like protease and 3C-like protease

(3CL^{pro}) [5,6]. Inhibition of the proteolytic processing can reduce viral replication and viral-induced cytotoxic effect [5,6]. The ability of coronaviruses to generate novel strains with high virulence through high frequency of mutations and recombination remains a potential threat to human health. Therefore, it is desirable to develop a broad-spectrum drug that can combat against all kinds of coronavirus infection. Because 3CL^{pro} is essential to viral replication and its active-site structure is conserved, the protease is an attractive drug target for the development of such a broad-spectrum inhibitor [7]. The SARS-CoV 3CL^{pro} can be inactivated by peptidomimetic inhibitors that are composed of a substrate-like peptide and a reactive warhead such as an aldehyde [8,9], a Michael acceptor [7,10,11], a halo-methyl ketone [10,12], or an epoxide [13]. The peptide interacts with the substrate-binding cleft of the protease to form a non-covalent complex, and then the warhead covalently links with the catalytic cysteine residue and inhibits the enzyme.

* Corresponding author. School of Life Sciences and Center for Protein Science and Crystallography, The Chinese University of Hong Kong, Rm 289 Science Centre, Shatin, Hong Kong. Tel.: +852 3943 8024; fax: +852 2603 7246.

E-mail address: kbwong@cuhk.edu.hk (K.-B. Wong).

In this study, we have shown that the nitrile group is an effective warhead against 3CL^{PRO}. Here, based on the auto-cleavage sequence of SARS-CoV 3CL^{PRO} (TSAVLQ↓), four nitrile-based inhibitors with different length of peptide sequences and protective groups were designed and synthesized. We have shown that these inhibitors were effective against 3CL^{PRO} from six different strains of CoVs with IC₅₀ values in the μM range. The crystal structures of the four enzyme–inhibitor complexes were determined to reveal the mechanism of inhibition and the enzyme–inhibitor interactions.

2. Results and discussion

2.1. SARS-CoV 3CL^{PRO} is inhibited by nitrile-based peptidomimetic inhibitors

Based on the autocleavage tetrapeptide sequence (AVLQ) of SARS-CoV 3CL^{PRO}, three nitrile-based inhibitors with different protective groups, 5-methylisoxazole-3-carboxyl (Mic), *tert*-butyloxycarbonyl (Boc) and carboxybenzyl (Cbz), were synthesized (Scheme 1). The protease activity in the presence of inhibitors was measured by using a fluorescent-protein substrate as described previously [14,15]. The IC₅₀ values of 'Mic-AVLQ-CN', 'Boc-AVLQ-CN', and 'Cbz-AVLQ-CN' were 49 ± 2, 49 ± 2, and 4.6 ± 0.2 μM, respectively (Fig. 1). Interestingly, the inhibitor with the Cbz protective group was ~10x more potent than the other inhibitors tested. To test the effect of increasing the length of the peptidomimetic inhibitor, we synthesized a hexapeptide inhibitor 'Cbz-TSAVLQ-CN'. The IC₅₀ value for this inhibitor was 39 ± 1 μM (Fig. 1), suggesting that increasing the length of the inhibitor did not improve inhibition and the Cbz group at the P4 position may be responsible for the higher potency of 'Cbz-AVLQ-CN'.

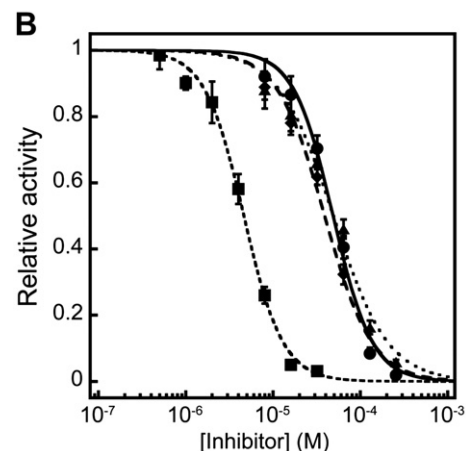
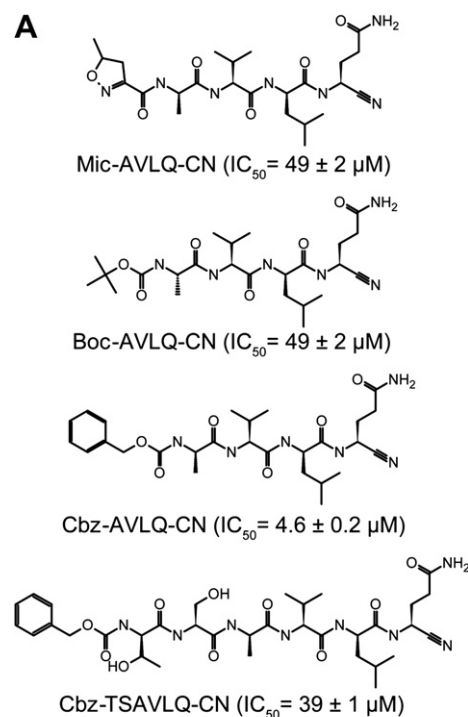
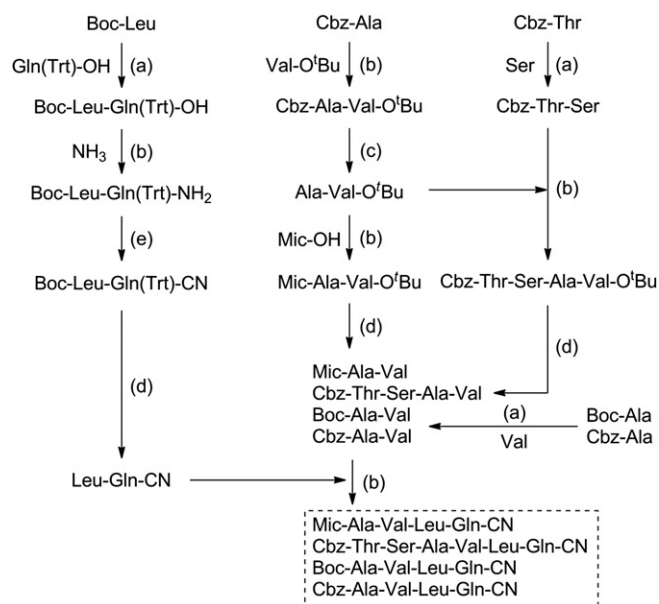


Fig. 1. IC₅₀ values of the nitrile-based inhibitors against SARS-CoV 3CL^{PRO}. (A) A schematic diagram shows chemical structures and IC₅₀ values of the inhibitors. (B) SARS-CoV 3CL^{PRO} was pre-mixed with 'Miu-AVLQ-CN' (circle), 'Boc-AVLQ-CN' (triangle), 'Cbz-AVLQ-CN' (square) and 'Cbz-TSAVLQ-CN' (diamond) at 0–256 μM, followed by measuring the protease activity to determine the inhibitory effect. The IC₅₀ values were determined by fitting the curve to a four-parameter logistics equation.

2.2. Crystal structures of enzyme–inhibitor complexes

To better understand the enzyme–inhibitor interaction, we determined the crystal structures of SARS-CoV 3CL^{PRO} in complex with the four inhibitors at 1.95–2.5 Å resolution (Table S1, Supplementary data). The 3CL^{PRO} formed a dimer in the crystal structure, and the inhibitors occupied the substrate binding site in both protomers. Electron density was observed for the tetrapeptide (Ala–Val–Leu–Gln) at P1 to P4 positions for all inhibitor complexes (Fig. S1, Supplementary material). Overlaying these inhibitor structures demonstrated that the tetrapeptides adopted the same conformation when bound to the 3CL^{PRO}. On the other hand, the protective group of 'Mic-AVLQ-CN', the P5-Ser and P6-Thr of 'Cbz-TSAVLQ-CN' were disordered and not observable in the electron density.



Scheme 1. Reaction scheme of nitrile-based peptidomimetic inhibitor synthesis. Step (a) was the coupling of peptides by using *N,N*-dicyclohexylcarbodiimide and *N*-hydroxysuccinimide. Step (b) was the coupling of peptides by the mixed anhydride method. Step (c) was the deprotection of benzyl carbamates by using palladium on charcoal. Step (d) was the deprotection of Boc, Trt, Pbf groups and tertiary butyl esters by using trifluoroacetic acid. Step (e) was the transformation of primary amide to nitrile by using trifluoroacetic anhydride. Final products were highlighted with dashed box.

In SARS-CoV, the catalytic dyad consists of Cys145 and His41 [16]. The inhibitor was covalently bonded with the thiol group of Cys145 via the carbon atom of the nitrile warhead (Fig. 2A). This mechanism is consistent with that observed in other cysteine proteases [17]. The side chains of P1-Gln, P2-Leu and P4-Ala occupied the S1, S2 and S4 subsites, respectively, of SARS-CoV 3CL^{Pro}, while the side-chain of P3-Val pointed towards the solvent (Fig. 2A). A number of hydrogen bonds are involved in enzyme–inhibitor interactions. The P1-Gln side chain was hydrogen-bonded with the backbone O atom of Phe140 and the side-chain of His163 and Glu166. The backbone amide groups of P2 to P4 formed hydrogen bonds with Glu166, Gln189 and Thr190, and these hydrogen bonds help the P3 and P4 residues to adopt a β -strand like conformation (Fig. 2B).

Noteworthy, the aromatic ring of the Cbz group is docked into a pocket where the ring can form favourable hydrophobic interactions with Pro168 and P3-Val (Fig. 2C). These extra interactions, which are absent in other enzyme–inhibitor complexes, may enhance the binding affinity between 3CL^{Pro} and increase the potency of the ‘Cbz-AVLQ-CN’ inhibitor.

2.3. Nitrile-based peptidomimetic inhibitor exhibits broad-spectrum inhibition against 3CL^{Pro} from different groups of coronaviruses

Next, we tested if the ‘Cbz-AVLQ-CN’ inhibitor has broad-spectrum inhibition against 3CL^{Pro} from different groups of coronaviruses. We measured and compared the IC₅₀ values of ‘Cbz-AVLQ-CN’ against 3CL^{Pro} from human coronavirus (HCoV) strains 229E (group 1), NL63 (group 1), OC43 (group 2a), HKU1 (group 2a), SARS-CoV (group 2b), and infectious bronchitis virus (IBV) (group 3). Our results showed that ‘Cbz-AVLQ-CN’ can inhibit all 3CL^{Pro} tested, with values of IC₅₀ ranging from 1.3 to 4.6 μ M (Fig. 3). In contrast, the ‘Cbz-AVLQ-CN’ had no observable inhibition effect on caspase-3 at 0.5–256 μ M (Fig. S2, Supplementary material), suggesting that the inhibitor is specific for 3CL^{Pro} from coronaviruses. As structures of 3CL^{Pro} from group 1, 2a, 2b, and 3 are similar, our modelling study suggests that the ‘Cbz-AVLQ-CN’ inhibitor can fit nicely to the active site of 3CL^{Pro} from all groups of coronaviruses and inhibit the protease via the same mechanism (Fig. S3, Supplementary material).

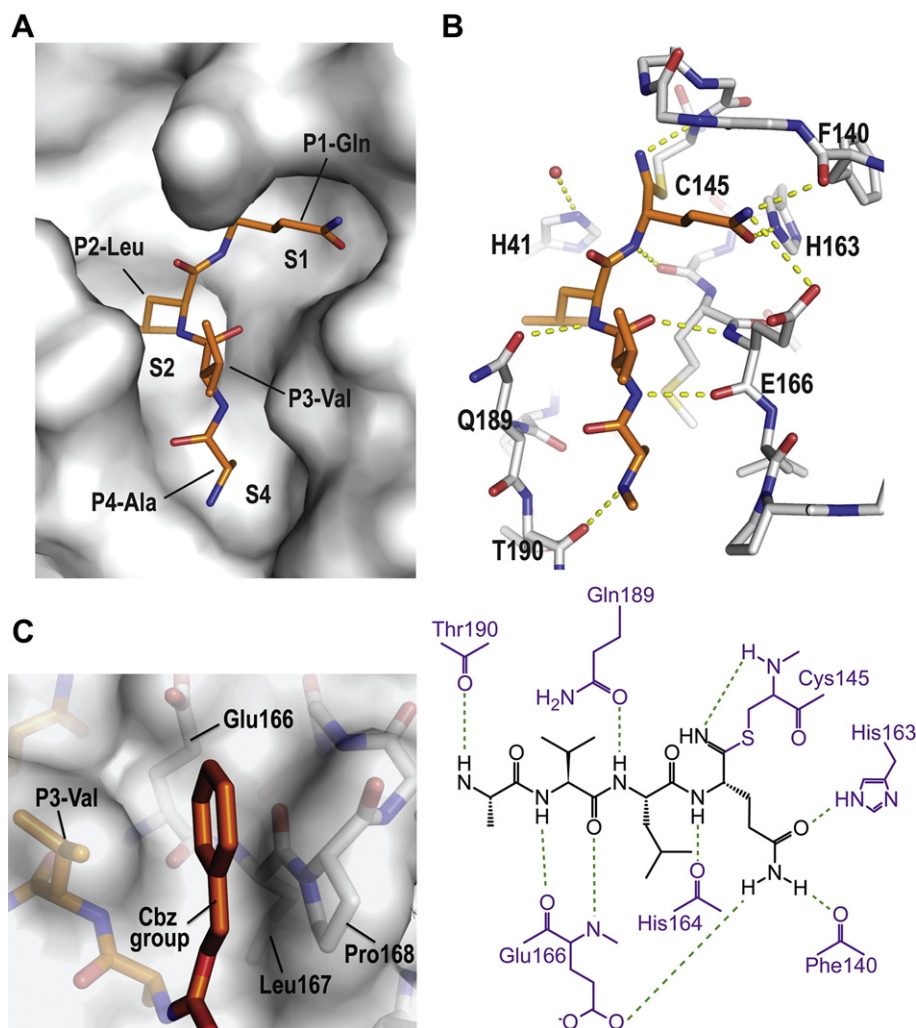


Fig. 2. Crystal structure of 3CL^{Pro}-inhibitor complex. (A) The 3CL^{Pro} was shown in surface representation, while the inhibitor was shown in stick representation. The side-chains of P1-Gln, P2-Leu and P4-Ala occupy the S1, S2, S4 subsites of 3CL^{Pro}, while the side-chain of P3-Val points towards the solvent. (B) The hydrogen bonds (dotted lines) between the inhibitor (orange) and the 3CL^{Pro} (grey) were shown. (C) The Cbz protective group of the ‘Cbz-AVLQ-CN’ docks into a pocket formed by Glu166, Leu167, and Pro168 of SARS-CoV 3CL^{Pro}. Surface was shown for atoms of 3CL^{Pro} and P1-P4 residues of the inhibitors. (For interpretation of the references to colour in this figure legend, the reader is referred to the web version of this article.)

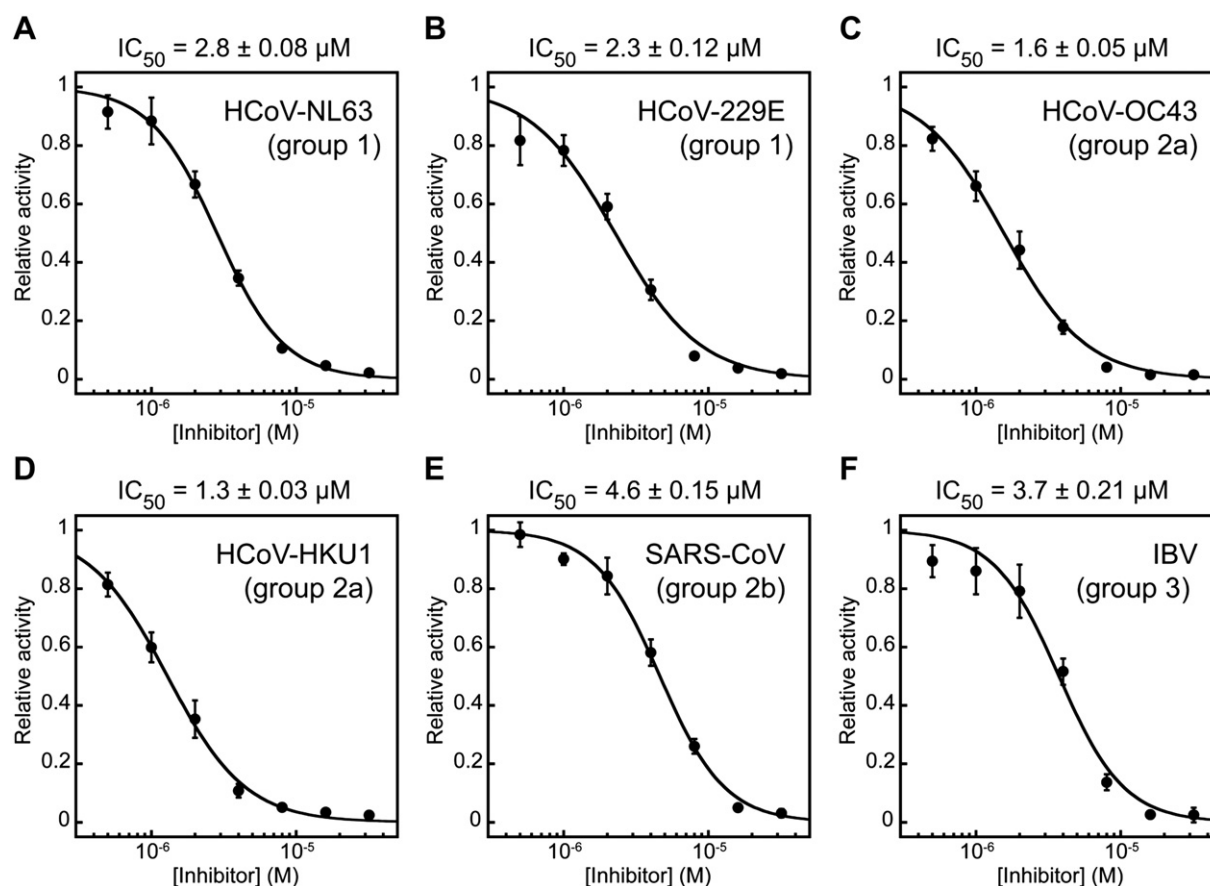


Fig. 3. Broad-spectrum inhibition of 'Cbz-AVLQ-CN' against 3CL^{pro} from (A) HCoV-NL63, (B) HCoV-229E, (C), HCoV-OC43, (D) HCoV-HKU1, (E) SARS-CoV, and (F) IBV. The proteases were pre-mixed with 'Cbz-AVLQ-CN' at 0–32 μM. The IC₅₀ values were determined by fitting the curve to a four-parameter logistics equation.

3. Conclusion

In this study, we have shown that nitrile-based peptidomimetic inhibitors display broad-spectrum inhibition against 3CL^{pro} from all groups of coronaviruses. Crystal structures of enzyme–inhibitor complexes provide interesting insights in the design of peptidomimetic inhibitors. First, the enzyme–inhibitor binding is mainly determined by the tetrapeptide sequence, AVLQ. This suggestion is consistent with the observation that extending the length of the inhibitor to hexapeptide ('Cbz-TSAVLQ-CN') did not improve inhibition (Fig. 1). Second, we found that the Cbz protective group at the N-terminus of the tetrapeptide can result in ~10 fold increases in potency in the 'Cbz-AVLQ-CN' inhibitor than the other inhibitors tested. This observation suggests that modification of the peptidomimetics, e.g. cross-linking the P3-Val with the Cbz groups, may further improve the efficacy of inhibition. Because of the high recombination frequency among the RNA genome of CoVs, development of a broad-spectrum inhibitor is an attractive strategy to combat against infection of all kinds of CoVs [7]. Here, we have shown that the nitrile-based inhibitor 'Cbz-AVLQ-CN' can inhibit 3CL^{pro} from all groups of CoVs tested with IC₅₀ values in the μM range. As nitrile-based protease inhibitors (e.g. odanacatib [18], vildagliptin [19]) have been successful in clinical applications [20], our work demonstrated that the inhibitors described in this study may serve as a lead for the development of antiviral drugs that target a broad-spectrum of coronaviruses.

4. Experimental section

4.1. Inhibitor synthesis

The reaction scheme for inhibitor synthesis is summarized in Scheme 1. 5-Methylisoxazole-3-carboxylic acid (Mic-OH), N,N'-dicyclohexylcarbodiimide (DCC), N-hydroxysuccinimide (HOSu) were purchased from Sigma–Aldrich. Identities of the final products were verified by ¹H nuclear magnetic resonance and mass spectrometry analysis.

4.1.1. Peptide coupling using N,N'-dicyclohexylcarbodiimide (DCC) and N-hydroxysuccinimide (HOSu)

In part 1, to a stirred suspension of N-protected-amino acid-OH or N-protected-peptide-OH (1.0 equiv) and HOSu (1.1 equiv) in anhydrous tetrahydrofuran (THF) (20 mL/mmol), DCC (1.1 equiv) in THF was added to the solution at 0 °C. The reaction mixture was stirred for 30 min at the same temperature and 6 h at 25 °C. N,N'-dicyclohexylurea was then removed by filtration and the filtrate was collected. In part 2, the amino acid was dissolved in THF/H₂O (v/v = 1:1), then the pH of the solution was adjusted to 9 with 2 M K₂CO₃. The filtrate from part 1 was added to the solution at 0 °C. This mixture was stirred for 30 min at 0 °C and overnight at 25 °C. Solvents were then evaporated *in vacuo* and the pH of the residue was adjusted to acidic with citric acid at 0 °C and extracted with ethyl acetate (EtOAc). The combined extracts were washed with brine, dried (MgSO₄), filtered and evaporated *in vacuo*. The residue

was purified by flash chromatography on silica gel to give the desired compound.

4.1.2. Peptide coupling using mixed anhydride method

N-protected-amino acid-OH or N-protected-peptide-OH (1 equiv) was dissolved in THF and cooled to -15°C . To the stirred solution, N-methylmorpholine (NMM) (1 equiv) and isobutylchloroformate (1 equiv) were added consecutively. After precipitation of N-methylmorpholine hydrochloride, the amine (1 equiv) was added and the mixture was allowed to warm to 25°C within 30 min. It was stirred for additional 90 min, and the solvent was removed under reduced pressure. The residue was dissolved in EtOAc and the solution was washed with H_2O , saturated NaHCO_3 , 5% citric acid and brine. The solvent was dried (MgSO_4) and evaporated. The crude residue was purified by flash column chromatography to give the product.

4.1.3. Deprotection of benzyl carbamates using palladium on charcoal (Pd/C)

To a stirred solution of the benzyl carbamate (1.0 equiv) in MeOH, palladium on charcoal (benzyl carbamate/palladium on charcoal = 1 g/100 mg) was added. The solution was evacuated, placed under H_2 (1 atm), and stirred for 1 h. The reaction was monitored by thin layer chromatography (TLC). The suspension was then filtered through Celite and washed with MeOH. The filtrate was concentrated under reduced pressure to afford the desired amine.

4.1.4. Deprotection of Boc, Trt groups and tertiary butyl esters using trifluoroacetic acid (TFA)

To a stirred solution of the starting materials (1.0 equiv) in CH_2Cl_2 , TFA (16.0 equiv) was added. The solution was stirred at 25°C and monitored by TLC. The CH_2Cl_2 /TFA solvent was removed under reduced pressure. The residue was diluted with toluene and the solvent was removed once again under reduced pressure.

4.1.5. Transformation from primary amide to nitrile using trifluoroacetic anhydride

To a stirred cold solution (0°C) of the primary amide (1.0 equiv) in dry THF and Et_3N (2.2 equiv), trifluoroacetic anhydride (1.1 equiv) was added over 5 min. The solution was allowed to warm to 25°C . After 30 min, the reaction was quenched with H_2O . The THF was removed under reduced pressure, and the product was extracted with EtOAc. The combined extracts were washed with saturated NaHCO_3 , 5% citric acid and brine, dried (MgSO_4), filtered and evaporated *in vacuo*. The residue was purified by flash chromatography on silica gel to give the desired compound.

4.1.6. Identification of products by NMR and mass spectrometry

4.1.6.1. Mic-AVLQ-CN. After this compound was synthesized by following the procedure as described in Section 4.1.2, the product was purified by flash chromatography on silica gel to afford the target compound (yield = 64%). R_f : 0.7 (EtOAc/MeOH = 4/1).

^1H NMR (300 MHz, d_6 -DMSO) δ (ppm): 0.50–1.08 (12H, m, $\text{CH}(\text{CH}_3)_2$), 1.30 (3H, d, $J = 6.8$ Hz, CH_3), 1.46–1.49 (2H, m, CH_2), 1.52–1.67 (1H, m, CH), 1.74–1.86 (1H, m, CH), 1.88–2.15 (2H, m, CH_2), 2.23–2.42 (2H, m, CH_2CONH_2), 2.46 (3H, s, $\text{CH}_3\text{C}=\text{CH}$), 3.96–4.40 (3H, m, NHCH), 4.42–4.65 (1H, m, NHCH), 6.56 (1H, s, $\text{C}=\text{CH}$), 7.03 (1H, s, NH), 7.26 (1H, s, NH), 7.94 (2H, d, $J = 8.4$ Hz, NH), 8.08 (1H, d, $J = 7.2$ Hz, NH), 8.62 (1H, d, $J = 7.2$ Hz, NH); ESI-HRMS (m/z): calculated for $\text{C}_{24}\text{H}_{37}\text{N}_7\text{O}_6 + \text{Na}^+$: 542.2703, found: 542.2706.

4.1.6.2. Boc-AVLQ-CN. After this compound was synthesized by following the procedure as described in Section 4.1.2, the product

was purified by flash chromatography on silica gel to afford the target compound (yield = 67%). R_f : 0.1 (EtOAc).

^1H NMR (300 MHz, d_6 -DMSO) δ (ppm): 0.68–0.96 (12H, m, $\text{CH}(\text{CH}_3)_2$), 1.15 (3H, d, $J = 6.9$ Hz, CH_3), 1.37 (9H, s, $\text{C}(\text{CH}_3)_3$), 1.41–1.52 (2H, m, CH_2), 1.52–1.66 (1H, m, CH), 1.67–1.87 (1H, m, CH), 1.87–2.09 (2H, m, CH_2), 2.33–2.49 (2H, m, CH_2CO), 3.86–4.04 (1H, m, NHCH), 4.06–4.33 (3H, m, NHCH), 7.09 (1H, d, $J = 7.5$ Hz, NH), 7.17 (1H, s, NH), 7.32 (1H, s, NH), 7.60 (1H, d, $J = 8.7$ Hz, NH), 7.93 (1H, d, $J = 8.1$ Hz, NH), 8.06 (1H, d, $J = 7.8$ Hz, NH). ESI-HRMS (m/z): calculated for $\text{C}_{24}\text{H}_{42}\text{N}_6\text{O}_6 + \text{Na}^+$: 533.3058, found: 533.2850.

4.1.6.3. Cbz-AVLQ-CN. After this compound was synthesized by following the procedure as described in Section 4.1.2, the product was purified by flash chromatography on silica gel to afford the target compound (yield = 73%). R_f : 0.65 ($\text{CH}_2\text{Cl}_2/\text{MeOH} = 1/4$).

^1H NMR (300 MHz, d_6 -DMSO) δ (ppm): 0.62–1.00 (12H, m, $\text{CH}(\text{CH}_3)_2$), 1.18 (3H, d, $J = 6.9$ Hz, CHCH_3), 1.20–1.30 (1H, m, CH_2), 1.32–1.52 (2H, m, CH_2), 1.52–1.66 (1H, m, CH), 1.66–1.86 (1H, m, $\text{CH}(\text{CH}_3)_2$), 1.86–2.14 (2H, m, CH_2CONH_2), 2.30–2.46 (1H, m, $\text{CH}(\text{CH}_3)_2$), 4.00–4.18 (2H, m, NHCH), 4.18–4.36 (2H, m, NHCH), 5.01 (2H, s, ArCH_2), 7.18 (1H, s, NH), 7.20–7.44 (6H, ArH, NH), 7.53 (1H, d, $J = 7.5$ Hz, NH), 7.77 (1H, d, $J = 8.7$ Hz, NH), 7.94 (1H, d, $J = 8.1$ Hz, NH), 8.05 (1H, d, $J = 7.5$ Hz, NH). ESI-HRMS (m/z): calculated for $\text{C}_{27}\text{H}_{40}\text{N}_6\text{O}_6 + \text{Na}^+$: 567.2907, found: 567.2902.

4.1.6.4. Cbz-TSAVLQ-CN. After this compound was synthesized by following the procedure as described in Section 4.1.2., the product was purified by flash chromatography on silica gel to afford the target compound (yield = 48%). R_f : 0.75 (MeOH/EtOAc = 3/1).

^1H NMR (300 MHz, d_6 -DMSO) δ (ppm): 0.68–0.96 (12H, m, $\text{CH}(\text{CH}_3)_2$), 1.06 (3H, d, $J = 6.3$ Hz, CHCH_3), 1.21–1.32 (4H, m, CH_3 , CH), 1.36–1.53 (2H, m, CH_2), 1.53–1.68 (1H, m, CHH), 1.68–1.88 (1H, m, CHH), 1.88–2.12 (2H, m, CH_2CONH_2), 2.33–2.46 (1H, m, CH), 3.44–3.70 (2H, m, CH_2OH), 3.84–4.00 (1H, m, CH_3CHOH), 4.00–4.14 (2H, m, NHCH), 4.14–4.40 (4H, m, NHCH), 4.92–4.94 (1H, m, OH), 4.96–5.13 (3H, m, ArCH_2 , OH), 7.02 (1H, d, $J = 8.1$ Hz, NH), 7.16 (1H, s, NH), 7.26 (1H, s, NH), 7.28–7.44 (5H, m, ArH), 7.73 (1H, d, $J = 8.1$ Hz, NH), 7.85 (1H, d, $J = 8.1$ Hz, NH), 7.89–8.02 (2H, m, NH), 8.13 (1H, d, $J = 6.9$ Hz, NH). ESI-HRMS (m/z): calculated for $\text{C}_{34}\text{H}_{52}\text{N}_8\text{O}_{10} + \text{Na}^+$: 755.3698, found: 755.3669.

4.2. Protease assay and determination of IC_{50} values

The detailed procedures for the production of 3CL^{PRO} , fluorescent substrate, and protease assay for 3CL^{PRO} were described previously [14,15]. 3CL^{PRO} at 0.5–1 μM were pre-mixed with 0.5–256 μM of inhibitors for 5 min, followed by addition of 35 μM substrate. The decay of fluorescence at 530 nm was fitted to a single-exponential decay to yield the observed rate constant (k_{obs}) and $k_{\text{obs}}/[3\text{CL}^{\text{PRO}}]$. The values of $k_{\text{obs}}/[3\text{CL}^{\text{PRO}}]$ at different concentration of inhibitors were normalized by those without inhibitors to determine the relative protease activities, which were fitted to a four-parameter logistics equation to obtain the IC_{50} values.

4.3. Structure determination of protease-inhibitor complexes

SARS-CoV 3CL^{PRO} was crystallized at 16°C using the hanging-drop-vapour-diffusion method by mixing 5 mg/mL 3CL^{PRO} in 1:1 ratio with 50 mM 2-(*N*-morpholino)ethanesulfonic acid, pH 5.5, 8.5% (w/v) polyethylene glycol 6000, 10% (v/v) glycerol, 3% (v/v) DMSO, 1 mM ethylenediaminetetraacetic acid and 1 mM dithiothreitol. Single crystals were transferred to 5 μL of the mother liquor with 600 μM inhibitors. After incubation at 16°C overnight, the crystals were cryoprotected by 20% (v/v) glycerol, and diffraction data were collected at 110 K in an in-house Rigaku FRE^+ X-ray

source. The phase was solved by molecular replacement, the models were built interactively by the program COOT [21] and refined by PHENIX [22].

Acknowledgements

This work was supported by the Research Fund for the Control of Infectious Diseases, Hong Kong SAR Government (project number: 06060432 and 09080282).

Appendix A. Supplementary data

Supplementary data related to this article can be found at <http://dx.doi.org/10.1016/j.ejmech.2012.10.053>.

References

- [1] P.C.Y. Woo, S.K.P. Lau, Y. Huang, K.-Y. Yuen, Coronavirus diversity, phylogeny and interspecies jumping, *Exp. Biol. Med.* 234 (2009) 1117–1127.
- [2] E.J. Snijder, P.J. Bredenbeek, J.C. Dobbe, V. Thiel, J. Ziebuhr, L.L. Poon, Y. Guan, M. Rozanov, W.J. Spaan, A.E. Gorbalenya, Unique and conserved features of genome and proteome of SARS-coronavirus, an early split-off from the coronavirus group 2 lineage, *J. Mol. Biol.* 331 (2003) 991–1004.
- [3] S.R. Dominguez, C.C. Robinson, K.V. Holmes, Detection of four human coronaviruses in respiratory infections in children: a one-year study in Colorado, *J. Med. Virol.* 81 (2009) 1597–1604.
- [4] E.R. Gaunt, A. Hardie, E.C. Claas, P. Simmonds, K.E. Templeton, Epidemiology and clinical presentations of the four human coronaviruses 229E, HKU1, NL63, and OC43 detected over 3 years using a novel multiplex real-time PCR method, *J. Clin. Microbiol.*, 48 2940–2947.
- [5] P.A. Rota, M.S. Oberste, S.S. Monroe, W.A. Nix, R. Campagnoli, J.P. Icenogle, S. Penaranda, B. Bankamp, K. Maher, M.H. Chen, S. Tong, A. Tamin, L. Lowe, M. Frace, J.L. DeRisi, Q. Chen, D. Wang, D.D. Erdman, T.C. Peret, C. Burns, T.G. Ksiazek, P.E. Rollin, A. Sanchez, S. Liffick, B. Holloway, J. Limor, K. McCaustland, M. Olsen-Rasmussen, R. Fouchier, S. Gunther, A.D. Osterhaus, C. Drosten, M.A. Pallansch, L.J. Anderson, W.J. Bellini, Characterization of a novel coronavirus associated with severe acute respiratory syndrome, *Science* 300 (2003) 1394–1399.
- [6] M.A. Marra, S.J. Jones, C.R. Astell, R.A. Holt, A. Brooks-Wilson, Y.S. Butterfield, J. Khattri, J.K. Asano, S.A. Barber, S.Y. Chan, A. Cloutier, S.M. Coughlin, D. Freeman, N. Girn, O.L. Griffith, S.R. Leach, M. Mayo, H. McDonald, S.B. Montgomery, P.K. Pandoh, A.S. Petrescu, A.G. Robertson, J.E. Schein, A. Siddiqui, D.E. Smailus, J.M. Stott, G.S. Yang, F. Plummer, A. Andonov, H. Artsob, N. Bastien, K. Bernard, T.F. Booth, D. Bowness, M. Czub, M. Drebot, L. Fernando, R. Flick, M. Garbutt, M. Gray, A. Grolla, S. Jones, H. Feldmann, A. Meyers, A. Kabani, Y. Li, S. Normand, U. Stroher, G.A. Tipples, S. Tyler, R. Vogrig, D. Ward, B. Watson, R.C. Brunham, M. Kraiden, M. Petric, D.M. Skowronski, C. Upton, R.L. Roper, The genome sequence of the SARS-associated coronavirus, *Science* 300 (2003) 1399–1404.
- [7] H. Yang, W. Xie, X. Xue, K. Yang, J. Ma, W. Liang, Q. Zhao, Z. Zhou, D. Pei, J. Ziebuhr, R. Hilgenfeld, K.Y. Yuen, L. Wong, G. Gao, S. Chen, Z. Chen, D. Ma, M. Bartlam, Z. Rao, Design of wide-spectrum inhibitors targeting coronavirus main proteases, *PLoS Biol.* 3 (2005) e324.
- [8] S. Yang, S.J. Chen, M.F. Hsu, J.D. Wu, C.T. Tseng, Y.F. Liu, H.C. Chen, C.W. Kuo, C.S. Wu, L.W. Chang, W.C. Chen, S.Y. Liao, T.Y. Chang, H.H. Hung, H.L. Shr, C.Y. Liu, Y.A. Huang, L.Y. Chang, J.C. Hsu, C.J. Peters, A.H. Wang, M.C. Hsu, Synthesis, crystal structure, structure-activity relationships, and antiviral activity of a potent SARS coronavirus 3CL protease inhibitor, *J. Med. Chem.* 49 (2006) 4971–4980.
- [9] K. Akaji, H. Konno, H. Mitsui, K. Teruya, Y. Shimamoto, Y. Hattori, T. Ozaki, M. Kusunoki, A. Sanjoh, Structure-based design, synthesis, and evaluation of peptide-mimetic SARS 3CL protease inhibitors, *J. Med. Chem.* 54 (2011) 7962–7973.
- [10] B.D. Santarsiero, W. Fu, B.H. Harcourt, P.A. Rota, S.C. Baker, M.E. Johnson, A.D. Mesecar, Design and synthesis of peptidomimetic severe acute respiratory syndrome chymotrypsin-like protease inhibitors, *J. Med. Chem.* 48 (2005) 6767–6771.
- [11] J.-j. Shie, J.-m. Fang, T.-h. Kuo, C.-j. Kuo, P.-h. Liang, H.-j. Huang, Y.-t. Wu, J.-t. Jan, Y.-s.E. Cheng, C.-h. Wong, Inhibition of the severe acute respiratory syndrome 3CL protease by peptidomimetic α,β -unsaturated esters, *Bioorg. Med. Chem.* 13 (2005) 5240–5252.
- [12] Y.-M. Shao, W.-B. Yang, T.-H. Kuo, K.-C. Tsai, C.-H. Lin, A.-S. Yang, P.-H. Liang, C.-H. Wong, Design, synthesis, and evaluation of trifluoromethyl ketones as inhibitors of SARS-CoV 3CL protease, *Bioorg. Med. Chem.* 16 (2008) 4652–4660.
- [13] T.W. Lee, M.M. Cherney, C. Huitema, J. Liu, K.E. James, J.C. Powers, L.D. Eltis, M.N. James, Crystal structures of the main peptidase from the SARS coronavirus inhibited by a substrate-like aza-peptide epoxide, *J. Mol. Biol.* 353 (2005) 1137–1151.
- [14] C.P. Chuck, L.T. Chong, C. Chen, H.F. Chow, D.C. Wan, K.B. Wong, Profiling of substrate specificity of SARS-CoV 3CL^{pro}, *PLoS ONE* 5 (2010) e13197.
- [15] C.-P. Chuck, H.-F. Chow, D.C.-C. Wan, K.-B. Wong, Profiling of substrate specificities of 3C-like proteases from group 1, 2a, 2b, and 3 coronaviruses, *PLoS ONE* 6 (2011) e27228.
- [16] C. Huang, P. Wei, K. Fan, Y. Liu, L. Lai, 3C-like proteinase from SARS coronavirus catalyzes substrate hydrolysis by a general base mechanism, *Biochemistry* 43 (2004) 4568–4574.
- [17] E. Dufour, A.C. Storer, R. Menard, Peptide aldehydes and nitriles as transition state analog inhibitors of cysteine proteases, *Biochemistry* 34 (1995) 9136–9143.
- [18] J.a. Eisman, H.G. Bone, D.J. Hosking, M.R. McClung, I.R. Reid, R. Rizzoli, H. Resch, N. Verbruggen, C.M. Hustad, C. DaSilva, R. Petrovic, A.C. Santora, B.A. Ince, A. Lombardi, Odanacatib in the treatment of postmenopausal women with low bone mineral density: three-year continued therapy and resolution of effect, *J. Bone Miner. Res.* 26 (2011) 242–251.
- [19] E.B. Villhauer, J.a. Brinkman, G.B. Naderi, B.F. Burkey, B.E. Dunning, K. Prasad, B.L. Mangold, M.E. Russell, T.E. Hughes, 1-[[[3-hydroxy-1-adamantyl]amino] acetyl]-2-cyano-(S)-pyrrolidine: a potent, selective, and orally bioavailable dipeptidyl peptidase IV inhibitor with antihyperglycemic properties, *J. Med. Chem.* 46 (2003) 2774–2789.
- [20] J. Wijkman, J. Gossen, Inhibitors of cathepsin K: a patent review (2004–2010), *Expert Opin. Ther. Pat.* 21 (2011) 1611–1629.
- [21] P. Emsley, B. Lohkamp, W.G. Scott, K. Cowtan, Features and development of coot, *Acta Crystallogr. D* 66 (2010) 486–501.
- [22] P.D. Adams, P.V. Afonine, G. Bunkoczi, V.B. Chen, I.W. Davis, N. Echols, J.J. Headd, L.W. Hung, G.J. Kapral, R.W. Grosse-Kunstleve, A.J. McCoy, N.W. Moriarty, R. Oeffner, R.J. Read, D.C. Richardson, J.S. Richardson, T.C. Terwilliger, P.H. Zwart, PHENIX: a comprehensive python-based system for macromolecular structure solution, *Acta Crystallogr. D* 66 (2010) 213–221.